nature genetics

Mutations in *TRPV4* cause Charcot-Marie-Tooth disease type 2C

Guida Landouré[1–4,12], Anselm A Zdebik[1,2,12], Tara L Martinez[5,6], Barrington G Burnett[3], Horia C Stanescu[1,2], Hitoshi Inada[7], Yijun Shi[3], Addis A Taye[3], Lingling Kong[5], Clare H Munns[8,9], Shelly S Choo[7], Christopher B Phelps[7], Reema Paudel[10], Henry Houlden[10], Christy L Ludlow[11], Michael J Caterina[8,9], Rachelle Gaudet[7], Robert Kleta[1,2,13], Kenneth H Fischbeck[3,13] & Charlotte J Sumner[5,13]

Charcot-Marie-Tooth disease type 2C (CMT2C) is an autosomal dominant neuropathy characterized by limb, diaphragm and laryngeal muscle weakness. Two unrelated families with CMT2C showed significant linkage to chromosome 12q24.11. We sequenced all genes in this region and identified two heterozygous missense mutations in the *TRPV4* gene, C805T and G806A, resulting in the amino acid substitutions R269C and R269H. TRPV4 is a well-known member of the TRP superfamily of cation channels. In TRPV4-transfected cells, the CMT2C mutations caused marked cellular toxicity and increased constitutive and activated channel currents. Mutations in *TRPV4* were previously associated with skeletal dysplasias. Our findings indicate that *TRPV4* mutations can also cause a degenerative disorder of the peripheral nerves. The CMT2C-associated mutations lie in a distinct region of the TRPV4 ankyrin repeats, suggesting that this phenotypic variability may be due to differential effects on regulatory protein-protein interactions.

Motor and sensory peripheral nerve cells are highly specialized, with long axons that connect the spinal cord with the periphery. Like all neurons, these cells are excitable and depend on ion channels for multiple functions, including action-potential propagation, synaptic transmission, plasticity and cell survival. Charcot-Marie-Tooth (CMT) disease (or hereditary motor and sensory neuropathy, HMSN) is a heterogeneous group of degenerative peripheral nerve disorders that together constitute the most common inherited neurological disease, with an incidence of 1 in 2,500 (ref. 1). In CMT, progressive axonal degeneration and cell death result in disabling muscle weakness and sensory loss.

We examined subjects from two large families with CMT type 2C (CMT2C) (**Table 1** and **Fig. 1a–f**), one of which was previously reported[2]. As described in prior studies[2–4], affected individuals showed evidence of a motor greater than sensory axonal neuropathy, causing progressive weakness of distal limb, diaphragm and laryngeal muscles (**Table 1**). Few affected individuals complained of sensory loss, but all had reduced or absent tendon reflexes. The age of onset and severity of disease were highly variable (**Table 1** and **Fig. 1a**). Most affected individuals reported a worsening of hand weakness in the cold. Bilateral sensorineural hearing loss was documented in ten subjects, and nine subjects complained of bladder urgency and incontinence. Muscle and nerve biopsies in a severely affected individual showed marked neurogenic atrophy of the gastrocnemius muscle, indicating severe loss of muscle innervations (**Fig. 1b**) and modest loss of sensory axons in the sural nerve with rare axons undergoing degeneration (**Fig. 1c–e**).

Fine mapping analysis in both families showed significant linkage to chromosome 12q24.11–12q24.21 ($\log_{10}$ of odds (lod) scores 3.1 and 6.9, respectively), confirming the findings of previous studies[4,5]. Haplotype reconstruction matched the disease status in all clinically affected subjects. Two individuals in family 1 carried the disease allele but were not found to be affected during limited examination in their homes. Combined data from families 1 and 2 narrowed the region of interest to a 2.6-Mb interval between the markers D12S105 and D12S1343 (**Fig. 1g**). SNP array analysis showed no duplications or deletions in this region (data not shown).

Sequencing of all 38 predicted protein-coding genes in the region of interest revealed heterozygous nucleotide variants C805T and G806A in exon 5 of the transient receptor potential vanilloid 4 (*TRPV4*) gene in affected family members of families 1 and 2, respectively (**Fig. 1h**). These sequence variants were not present

[1]Department of Medicine and [2]Department of Neuroscience, Physiology and Pharmacology, University College London, London, UK. [3]Neurogenetics Branch, National Institute of Neurological Disorders and Stroke (NINDS), National Institutes of Health (NIH), Bethesda, Maryland, USA. [4]Service de Neurologie, Centre Hospitalo-Universitaire du Point 'G', Université de Bamako, Bamako, Mali. [5]Department of Neurology, Johns Hopkins University, Baltimore, Maryland, USA. [6]W. Harry Feinstone Department of Molecular Microbiology and Immunology, Johns Hopkins Bloomberg School of Public Health, Baltimore, Maryland, USA. [7]Department of Molecular and Cellular Biology, Harvard University, Cambridge, Massachusetts, USA. [8]Department of Biological Chemistry and [9]Department of Neuroscience, Center of Sensory Biology, Johns Hopkins University, Baltimore, Maryland, USA. [10]University College London, Institute of Neurology, London, UK. [11]Laboratory of Neural Bases of Communication and Swallowing, James Madison University, Harrisonburg, Virginia, USA. [12]These authors contributed equally to this work. [13]These authors jointly directed the project. Correspondence should be addressed to C.J.S. (csumner1@jhmi.edu).

Received 5 October; accepted 3 December; published online 27 December 2009; doi:10.1038/ng.512

Table 1 Phenotypic characteristics of subjects with CMT2C

Patient	Age (yr)	Sex	Age of onset (yr)	First symptom	Vocal fold paresis	Limb weakness		Sensory loss	Hearing loss
						Proximal	Distal		
F1 III2	71	F	44	Foot weakness	Mild	None	Moderate	Minimal	Yes
F1 IV2	48	F	5	Foot weakness	Moderate	Mild	Severe	Mild	No
F1 IV3	46	F	5	Stridor	Moderate	Mild	Moderate	Mild	No
F1 IV4	44	F	3	Foot weakness	Severe	Severe	Severe	Moderate	Yes
F1 V1	24	F	7	Foot weakness	ND	None	Mild	Mild	No
F1 V3	20	F	5	Stridor	ND	None	Mild	Mild	No
F1 V8	18	M	2	Stridor	Severe	None	Mild	Minimal	No
F2 III11	65	M	57	Hearing loss	Mild	None	Mild	Minimal	Yes
F2 III18	61	M	34	Foot weakness	Mild	Mild	Moderate	Minimal	Yes
F2 III22	64	F	35	Foot weakness	Mild	Mild	Severe	Minimal	Yes
F2 III23	57	F	22	Foot weakness	Moderate	None	Mild	Minimal	Yes
F2 III24	49	F	<2	Stridor	Moderate	Mild	Moderate	Mild	Yes
F2 IV2	50	M	16	Hoarseness	Mild	Mild	Moderate	Mild	Yes
F2 IV5	53	M	28	Hoarseness	Moderate	None	Mild	Minimal	Yes
F2 IV9	31	F	5	Stridor	Moderate	None	Mild	None	No
F2 IV10	29	M	5	Hoarseness	Moderate	None	Mild	Minimal	Yes
F2 IV12	29	F	2	Stridor	Severe	Moderate	Severe	Mild	No

ND, not determined.

in 209 ethnically matched unaffected control individuals. The identified mutations predict substitutions at the same amino acid (R269C and R269H) in the TRPV4 protein. This residue is conserved across multiple vertebrate species (**Fig. 1i**). Sequencing of *TRPV4* in two other families with a CMT2C-like phenotype failed to identify any mutations, and in one, linkage to chromosome 12q24.11 was excluded, suggesting that CMT2C may be genetically heterogeneous (**Supplementary Fig. 1**).

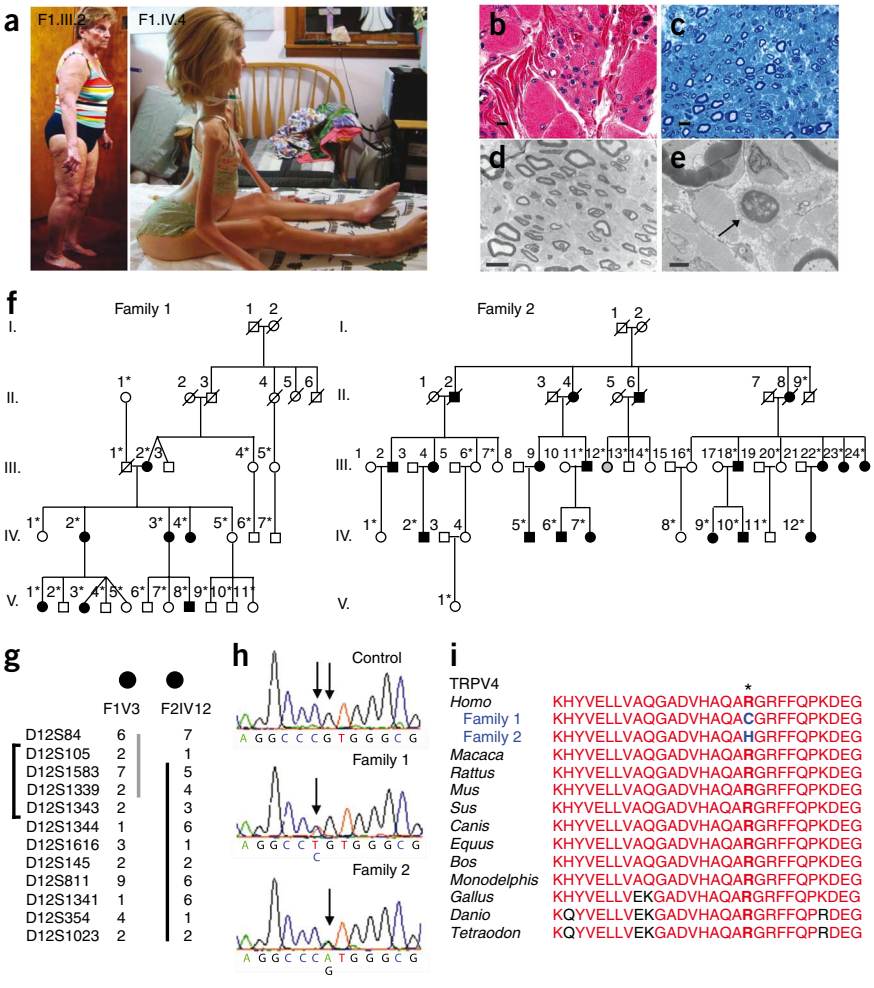

Figure 1 Phenotypic and genetic characteristics of CMT2C. (**a**) Marked variability of disease severity is demonstrated by mild, late-onset weakness in subject F1.III.2, but severe quadriparesis and respiratory failure in her daughter, subject F1.IV.4. Written consent was obtained to publish these photographs. (**b**) Light microscope images of hematoxylin and eosin-stained sections of gastrocnemius muscle biopsy from subject F1.IV.4 demonstrating profound denervation atrophy of muscle. Scale bar, 10 µm. (**c**) Toluidine blue–stained section of sural nerve shows mild loss of large, myelinated sensory axons. Scale bar, 10 µm. (**d**) Electron microscopy of sural nerve confirms mild loss of large and small myelinated axons and unmyelinated axons. Scale bar, 10 µm. (**e**) Arrow demonstrates a rare axon undergoing Wallerian-like axonal degeneration. Scale bar, 2 µm. (**f**) Pedigrees of families 1 and 2 demonstrating affected subjects in each of three generations. White, unaffected; black, affected; gray, unknown disease status. *Sample collected. (**g**) The haplotypes for subjects F1.V.3 and F2.IV.12 are shown. Family 1 defines the lower border (marker D12S1343) and family 2 defines the upper border (marker D12S105) of the region of interest. The bracket indicates the linked region. (**h**) Sequencing shows a heterozygous C805T change in family 1 and a G806A change in family 2 in *TRPV4*. (**i**) Protein homology of TRPV4 in various species. The mutations result in amino acid substitutions at Arg269, a highly conserved residue.

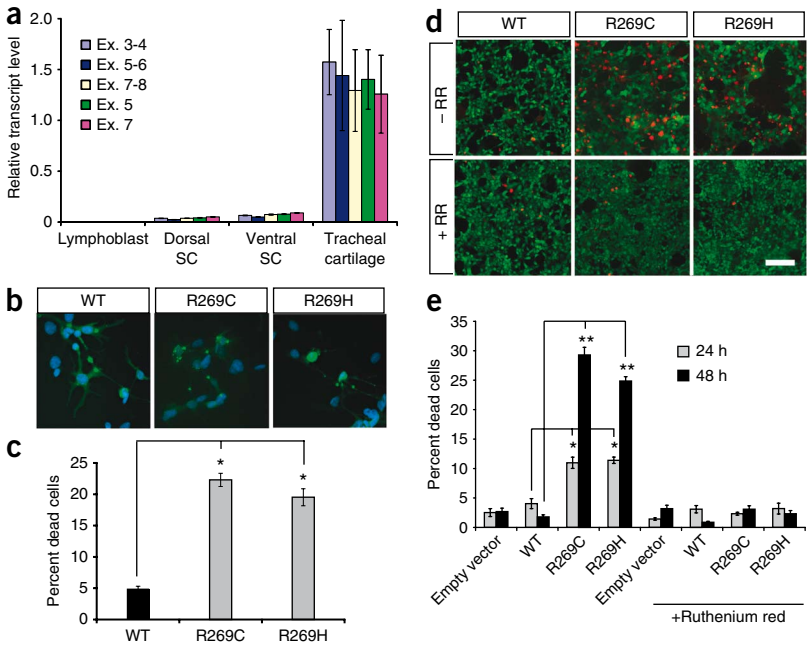

Figure 2 Mutant TRPV4 causes neuronal toxicity. (**a**) Quantification of *TRPV4* transcript by qRT-PCR in control human lymphoblast lines ($n = 4$), human dorsal spinal cord ($n = 3$), ventral spinal cord ($n = 3$) and tracheal cartilage ($n = 3$) using primers specific for the following exon regions: exons 3–4, exons 5–6, exons 7–8, exon 5 and exon 7. Values are normalized to the first tracheal cartilage sample. Data is averaged; error bars, s.e.m. (**b**) DRG neurons were transfected with wild-type and mutant forms of TRPV4 (green). At 16 h, some cells expressing mutant forms of TRPV4 show evidence of early cellular toxicity with a collapsed cytoplasm. The nuclear DAPI stain is blue. Scale bar, 40 μm. (**c**) Quantification of propidium iodide uptake in DRG neurons expressing wild-type and mutant TRPV4 reveals a marked increase of cell toxicity in mutant expressing cells at 48 h. $*P < 0.0001$. (**d**) HEK293 cells expressing R269C and R269H mutants show an increase in the number of dead cells (red channel is EthD-1 stain) at 48 h; this increase is prevented by the TRP channel blocker ruthenium red (RR). Green channel is calcein-AM stain for live cells. Scale bar, 200 μm. (**e**) Quantification of cell death in HEK293 cells indicates a time-dependent increase in cell death that is blocked by the TRP channel blocker ruthenium red (RR). $*P < 0.01$, $**P < 0.001$. Data in **c** and **e** are averaged from three independent experiments; error bars, s.e.m.

Mutations in *TRPV4* have been previously associated with skeletal dysplasias[6,7]. *TRPV4* was identified as the causative gene in these disorders in part due to high expression levels in cartilage compared to other tissue types[6]. TRPV4 has been reported to be expressed in motor neurons[8], ventral root[8] and dorsal root ganglion (DRG) neurons[9]. *In situ* hybridization studies show *Trpv4* mRNA expression in ventral and dorsal horn neurons of adult mouse spinal cord tissue (Allen Institute for Brain Science Spinal Cord Atlas; see URL section). We investigated Trpv4 protein expression in spinal cord tissue by immunohistochemistry (IHC) in Trpv4-null mice[10] and in wild-type littermates (**Supplementary Fig. 2**). These studies showed low levels of expression in motor neurons. We further quantified *TRPV4* expression levels in adult human tissues by quantitative reverse transcription PCR (qRT-PCR). Compared to tracheal cartilage, *TRPV4* was expressed at approximately 95% lower levels in dorsal and ventral human spinal cord (**Fig. 2a**). Although it has been suggested that there may be alternatively spliced isoforms of *TRPV4* lacking exon 5 and/or exon 7 (ref. 11), we detected no differential expression of such isoforms in spinal cord tissue (**Fig. 2a**).

Although TRPV4 was expressed at rather low levels in spinal neurons, mutant forms of TRPV4 were highly toxic to cultured neuronal cells. The CMT2C-associated mutant TRPV4 caused a fourfold increase in cell death in DRG neurons compared to wild-type TRPV4 at 48 h (**Fig. 2b**,**c**). We further evaluated toxicity in cells from the human embryonic kidney (HEK) 293 line (**Fig. 2d**,**e**). The R269C and R269H mutants caused a time-dependent increase in cell death, which was increased twofold at 24 h and approximately sixfold at 48 h. This was associated with increased intracellular calcium levels at 24 h (**Supplementary Fig. 3**). Notably, increased calcium levels and cell death were blocked by the TRP channel–inhibitor ruthenium red (**Fig. 2d**,**e** and **Supplementary Fig. 3**), by the specific TRPV4 inhibitor RN-1734[12] (**Supplementary Fig. 4**) and by the TRPV4 pore-inactivating substitution M680K[13] (**Supplementary Fig. 4**). Together, these data indicate that the cell death is due to aberrant activity of the TRPV4 channel.

TRPV4 is a nonselective cation channel that responds to environmental stimuli such as temperature, hypotonicity and chemicals including phorbol derivatives and arachidonic acid[14–20]. To investigate the effects of CMT2C-associated mutations on TRPV4 channel activity, we expressed wild-type and mutant TRPV4 in *Xenopus laevis* oocytes incubated in Ca^{2+}-free frog Ringer solution. Oocytes expressing the R269C and R269H mutants showed a 2.5-fold increase in channel currents compared to wild-type under resting conditions (18 °C) (**Fig. 3a**). Addition of ruthenium red at 10 μM reduced wild-type, R269H and R269C currents by 53%, 52% and 48%, respectively ($P < 0.05$). When the temperature was increased to 38 °C, both wild-type and mutant channel currents increased two- to threefold above their constitutive levels, with mutant channel currents remaining two- to threefold higher than wild-type currents (**Fig. 3a**). Similar results were obtained when the TRPV4 channels were activated by 4α-phorbol didecanoate (4αPDD) (**Fig. 3b**,**c**). Increasing the temperature in the oocytes pre-incubated with 4αPDD resulted in a further increase in channel activity (**Fig. 3b**,**c**). Higher basal currents and enhanced responses to both 4αPDD and hypotonic stimulation were also observed in HEK293 cells transfected with R269C or R269H mutants as compared to wild type (**Supplementary Fig. 5**). Increased channel activity could not be accounted for by changes in TRPV4 channel subcellular localization. Analysis of surface incorporation of TRPV4 by cell surface biotinylation assays showed approximately equal amounts of TRPV4 incorporated into the cell membrane (**Fig. 3d**). Furthermore, wild-type and mutant TRPV4 expressed in cells from the HeLa and HEK293 lines showed similar spatial distributions (**Supplementary Fig. 6**).

The TRPV4 protein has distinct domains, including six transmembrane segments with a putative ion pore region between S5 and S6, an intracellular N-terminal domain containing six ankyrin repeats and a C-terminal intracellular domain (**Fig. 4a**). Ankyrin repeats mediate protein-protein interactions, some of which have been shown to modulate TRPV4 activity[21]. The 2.3-Å crystal structure of the chicken Trpv4 ankyrin repeat domain (ARD) (**Fig. 4b** and **Supplementary Table 1**) shows a typical hand-shaped structure with a concave palm

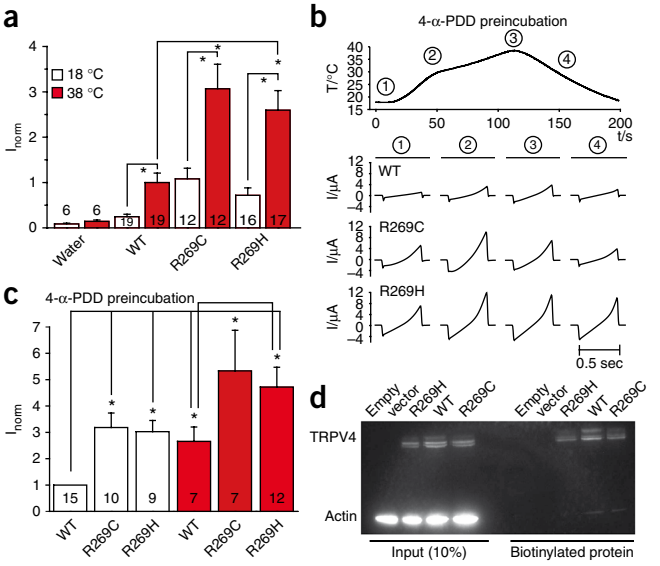

Figure 3 The R269C and R269H substitutions cause increased TRPV4 currents without a change in membrane localization. (**a**) Wild-type and mutant TRPV4 were expressed in *Xenopus* oocytes, and currents were measured at 18 °C and after heating to 38 °C. Currents obtained at −100 mV were normalized to currents in wild-type at 38 °C. Basal and stimulated channel activities of both mutants were significantly increased compared to wild-type ($P < 0.006$). Data are averaged from the number of experiments per condition shown in the columns; error bars, s.e.m. $^*P < 0.006$. (**b**) Representative current ramps obtained after preincubation in 5 μM 4αPDD (obtained from clamping cells from −100 to +100 mV in 500 ms). (**c**) Summary of the data obtained in **b**. Currents obtained at −100 mV were normalized to wild-type at 18 °C. $^*P < 0.05$. (**d**) Immunodetection of TRPV4 proteins shows appropriately sized bands for TRPV4 in 10% of whole cell extract inputs and the biotinylated fraction. There was no difference in the amount of wild-type compared to mutant TRPV4 in the membrane fraction (biotinylated fraction). Shown is one representative blot of four independent experiments.

surface formed by inner helices and fingers and a convex surface representing the back of the hand. Arg269 is located at the base of finger 3 on the convex surface, opposite the palm surface harboring previously described skeletal dysplasia mutations in the ARD[7] (**Fig. 4b**,**c**). Comparison with the TRPV1, TRPV2 and TRPV6 structures[22–24] shows that the backbone structure is conserved at this position, although the arginine residue is not conserved in other TRPV channels (data not shown). The R269C and R269H substitutions are thus unlikely to disrupt the protein fold, but the Arg269 side chain is exposed and well positioned to mediate protein-protein interactions that may be critical to TRPV4 function. Binding assays and co-immunoprecipitation experiments did not show changes in the interaction of mutant TRPV4 with two known protein partners, calmodulin[21] and PACSIN3[25] (**Supplementary Fig. 7**), confirming that the CMT2C-associated mutations do not grossly disrupt protein folding. Further experiments are needed to define whether specific intermolecular or intramolecular interactions are affected by the Arg269 substitution.

CMT2C is an unusual peripheral neuropathy resulting in motor greater than sensory axonal degeneration. Here we have shown that, despite low expression levels of TRPV4 in neurons, the CMT2C-associated TRPV4 alterations are highly toxic due to increased channel activity, causing calcium overload. Ca^{2+} is an essential intracellular signal in neurons regulating neurite outgrowth, synaptogenesis, synaptic transmission and plasticity, but excessive influx of Ca^{2+} has also long been associated with neurodegeneration[26]. Notably, many of the severely affected individuals in the families we studied had sensorineural hearing loss and bladder urgency (**Table 1**). Trpv4 knockout mice have been shown to have sensorineural hearing loss, impairment of bladder voiding and abnormalities of mechanosensation and nociception[10,27,28], indicating that some of the clinical manifestations of CMT2C may be attributable to a loss of normal TRPV4 function, as well as to the toxic effects of abnormal channel opening and calcium influx.

Mutations of *TRPV4* have been associated with autosomal dominant skeletal dysplasias. Brachyolmia is caused by R616Q and V620I substitutions, which increase basal and stimulated channel activity, perhaps via direct alteration of the S5 pore domain[6]. More recently, the D333G and I331F substitutions have been identified in the fifth ankyrin repeat in single individuals with spondylometaphyseal dysplasia Kozlowski type and metatropic dysplasia, respectively[7]. TRP channels operate within macromolecular complexes[29], and the ankyrin motifs are likely critical mediators of protein-protein interactions that regulate TRP channel localization and activity. The Arg269 residue localized to the convex face of the TRPV4-ARD may mediate distinct interactions with yet-to-be identified regulatory partners that are particularly important for TRPV4 function in peripheral neurons.

TRPV4 is a cation channel known to play a role in fundamental cellular processes such as osmosensation, temperature sensation and mechanosensation. In this study, we have shown that CMT2C

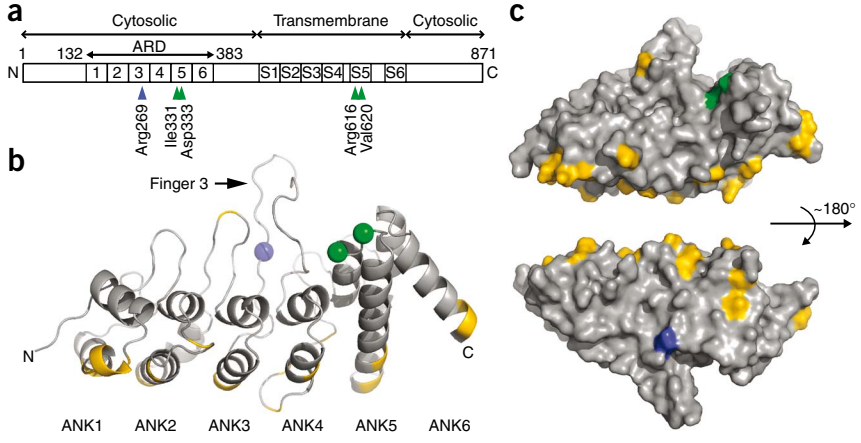

Figure 4 The R269C and R269H substitutions are located in the ankyrin repeat domain (ARD) of the TRPV4 protein. (**a**) Primary structure of the TRPV4 protein, with the positions of the CMT2C-associated (Arg269; blue arrowhead) and skeletal dysplasia–associated[6,7] (green arrowheads) mutations indicated below. (**b**) Ribbon diagram of the chicken Trpv4 ARD, with the location of the Arg269 residue (Arg255 in chicken sequence) depicted as a blue sphere and the Ile331 and Asp333 residues (Ile317 and Asp319 in chicken sequence, respectively) previously shown to be mutated in skeletal dysplasia as green spheres. (**c**) Surface representation of the TRPV4 ARD with Arg269 in blue and Ile331 and Asp333 in green. Residues that differ between chicken and human TRPV4 are yellow, demonstrating that the palm and finger regions are conserved.

is associated with substitutions at the Arg269 residue in the ARD of the TRPV4 protein. This work uncovers a previously unrecognized role for TRPV4 in neurons and highlights the importance of this ion channel in normal peripheral nerve function. Together with the observations that disruption of TRPML1 causes the central nervous system lysosomal-storage disease mucolipidosis type IV[30] and that mutation of Trpc3 causes degeneration of cerebellar neurons in mice[31], this study emphasizes the importance of TRP channels in the pathogenesis of neurodegenerative diseases. Most surprisingly, our data indicate that distinct alterations in this important ion channel result in strikingly different phenotypes that involve separate organ systems.

URLs. Allen Institute for Brain Science Spinal Cord Atlas: http://mousespinal.brain-map.org/imageseries/show.html?id=100017703.

METHODS

Methods and any associated references are available in the online version of the paper at http://www.nature.com/naturegenetics/.

Accession codes. Protein Data Bank: TRPV4 ankyrin repeat domain (TRPV4 $ARD_{132–383}$), 3JXI and 3JXJ (crystal forms I and II, respectively).

Note: Supplementary information is available on the Nature Genetics website.

ACKNOWLEDGMENTS

We are grateful to the subjects and their families for participating in this study. We thank J. Kissel for discussions regarding clinical evaluation of family 1, A. LaPean for aid in subject characterization, M. K. Floeter and T. Lehky for performing neurophysiological studies, R. R. Wang for crystallization and X-ray data collection, J. Hardy for helpful discussion regarding genetic analysis, A. Singleton and D. Hernandez for help with SNP array analysis, the NINDS DNA sequencing facility for help with sequencing, the Maryland Brain and Tissue Bank for providing human spinal cord and tracheal tissues, M. Suzuki for Trpv4 knockout mice, R. Tsien for providing the fluorescent protein mCherry, A. Hoke for providing DRG cells, J. Griffin for aid in nerve pathology evaluation, S. Heller for providing antibody to TRPV4, T. Jentsch for cells and instruments, C. Rojas and J. Alt for help with FLIPR, S. Minogue for assistance in confocal imaging, M.A. Valverde for providing human TRPV4 expression constructs and M. Plomann for providing PACSIN expression constructs and antibodies. This work was supported by intramural funds from the NINDS at NIH, funds from the Johns Hopkins Department of Neurology and the David and Elaine Potter Charitable Foundation, and NIH grant R01GM081340 and a McKnight Scholar Award to R.G.

AUTHOR CONTRIBUTIONS

C.J.S., K.H.F. and R.K. directed the study, and C.J.S wrote the paper. C.J.S., K.H.F., C.L.L., H.H. and G.L. evaluated subjects. R.K., H.C.S., K.H.F. and G.L. did the genetic analysis, and Y.S., A.A.T., R.P., R.K., K.H.F and G.L. carried out the gene sequencing. B.G.B., T.L.M., L.K. and C.J.S. performed qRT-PCR, IHC, cell death assays and co-IP experiments. A.A.Z. completed cell surface biotinylation and electrophysiology in *Xenopus* oocytes. H.I. and R.G. did electrophysiology in HEK cells and protein-binding assays. Protein structure determination was done by R.G., S.S.C. and C.B.P. Cell calcium imaging was completed by C.H.M. and M.J.C.

Published online at http://www.nature.com/naturegenetics/.
Reprints and permissions information is available online at http://npg.nature.com/reprintsandpermissions/.

1. Skre, H. Genetic and clinical aspects of Charcot-Marie-Tooth's disease. *Clin. Genet.* **6**, 98–118 (1974).
2. Dyck, P.J. *et al.* Hereditary motor and sensory neuropathy with diaphragm and vocal cord paresis. *Ann. Neurol.* **35**, 608–615 (1994).
3. Santoro, L. *et al.* Charcot-Marie-Tooth disease type 2C: a distinct genetic entity. Clinical and molecular characterization of the first European family. *Neuromuscul. Disord.* **12**, 399–404 (2002).
4. McEntagart, M.E. *et al.* Confirmation of a hereditary motor and sensory neuropathy IIC locus at chromosome 12q23–q24. *Ann. Neurol.* **57**, 293–297 (2005).
5. Klein, C.J. *et al.* The gene for HMSN2C maps to 12q23–24: a region of neuromuscular disorders. *Neurology* **60**, 1151–1156 (2003).
6. Rock, M.J. *et al.* Gain-of-function mutations in *TRPV4* cause autosomal dominant brachyolmia. *Nat. Genet.* **40**, 999–1003 (2008).
7. Krakow, D. *et al.* Mutations in the gene encoding the calcium-permeable ion channel TRPV4 produce spondylometaphyseal dysplasia, Kozlowski type and metatropic dysplasia. *Am. J. Hum. Genet.* **84**, 307–315 (2009).
8. Facer, P. *et al.* Differential expression of the capsaicin receptor TRPV1 and related novel receptors TRPV3, TRPV4 and TRPM8 in normal human tissues and changes in traumatic and diabetic neuropathy. *BMC Neurol.* **7**, 11 (2007).
9. Liedtke, W. *et al.* Vanilloid receptor-related osmotically activated channel (VR-OAC), a candidate vertebrate osmoreceptor. *Cell* **103**, 525–535 (2000).
10. Suzuki, M., Mizuno, A., Kodaira, K. & Imai, M. Impaired pressure sensation in mice lacking TRPV4. *J. Biol. Chem.* **278**, 22664–22668 (2003).
11. Arniges, M., Fernandez-Fernandez, J.M., Albrecht, N., Schaefer, M. & Valverde, M.A. Human TRPV4 channel splice variants revealed a key role of ankyrin domains in multimerization and trafficking. *J. Biol. Chem.* **281**, 1580–1586 (2006).
12. Vincent, F. *et al.* Identification and characterization of novel TRPV4 modulators. *Biochem. Biophys. Res. Commun.* **389**, 490–494 (2009).
13. Voets, T. *et al.* Molecular determinants of permeation through the cation channel TRPV4. *J. Biol. Chem.* **277**, 33704–33710 (2002).
14. Alessandri-Haber, N. *et al.* Hypotonicity induces TRPV4-mediated nociception in rat. *Neuron* **39**, 497–511 (2003).
15. Güler, A.D. *et al.* Heat-evoked activation of the ion channel, TRPV4. *J. Neurosci.* **22**, 6408–6414 (2002).
16. Watanabe, H. *et al.* Activation of TRPV4 channels (hVRL-2/mTRP12) by phorbol derivatives. *J. Biol. Chem.* **277**, 13569–13577 (2002).
17. Watanabe, H. *et al.* Anandamide and arachidonic acid use epoxyeicosatrienoic acids to activate TRPV4 channels. *Nature* **424**, 434–438 (2003).
18. Vriens, J. *et al.* Cell swelling, heat, and chemical agonists use distinct pathways for the activation of the cation channel TRPV4. *Proc. Natl. Acad. Sci. USA* **101**, 396–401 (2004).
19. Everaerts, W., Nilius, B. & Owsianik, G. The vallinoid transient receptor potential channel Trpv4: from structure to disease. *Prog. Biophys. Mol. Biol.* published online doi:10.1016/j.pbiomolbio.2009.10.002 (14 October 2009).
20. Liedtke, W. Molecular mechanisms of TRPV4-mediated neural signaling. *Ann. NY Acad. Sci.* **1144**, 42–52 (2008).
21. Phelps, C.B., Wang, R.R., Choo, S.S. & Gaudet, R. Differential regulation of TRPV1, TRPV3 and TRPV4 sensitivity through a conserved binding site on the ankyrin repeat domain. *J. Biol. Chem.* published online, doi:10.1074/jbc.M109.052548 (28 October 2009).
22. Jin, X., Touhey, J. & Gaudet, R. Structure of the N-terminal ankyrin repeat domain of the TRPV2 ion channel. *J. Biol. Chem.* **281**, 25006–25010 (2006).
23. Lishko, P.V., Procko, E., Jin, X., Phelps, C.B. & Gaudet, R. The ankyrin repeats of TRPV1 bind multiple ligands and modulate channel sensitivity. *Neuron* **54**, 905–918 (2007).
24. Phelps, C.B., Huang, R.J., Lishko, P.V., Wang, R.R. & Gaudet, R. Structural analyses of the ankyrin repeat domain of TRPV6 and related TRPV ion channels. *Biochemistry* **47**, 2476–2484 (2008).
25. Cuajungco, M.P. *et al.* PACSINs bind to the TRPV4 cation channel. PACSIN 3 modulates the subcellular localization of TRPV4. *J. Biol. Chem.* **281**, 18753–18762 (2006).
26. Mattson, M.P. Calcium and neurodegeneration. *Aging Cell* **6**, 337–350 (2007).
27. Tabuchi, K., Suzuki, M., Mizuno, A. & Hara, A. Hearing impairment in TRPV4 knockout mice. *Neurosci. Lett.* **382**, 304–308 (2005).
28. Gevaert, T. *et al.* Deletion of the transient receptor potential cation channel TRPV4 impairs murine bladder voiding. *J. Clin. Invest.* **117**, 3453–3462 (2007).
29. Clark, K., Middelbeek, J. & van Leeuwen, F.N. Interplay between TRP channels and the cytoskeleton in health and disease. *Eur. J. Cell Biol.* **87**, 631–640 (2008).
30. Venkatachalam, K. *et al.* Motor deficit in a *Drosophila* model of mucolipidosis type IV due to defective clearance of apoptotic cells. *Cell* **135**, 838–851 (2008).
31. Becker, E.B. *et al.* A point mutation in TRPC3 causes abnormal Purkinje cell development and cerebellar ataxia in moonwalker mice. *Proc. Natl. Acad. Sci. USA* **106**, 6706–6711 (2009).

ONLINE METHODS

Subjects. Subjects were enrolled in NINDS Institutional Review Board or University College London Research Ethics Committee approved protocols. Informed consent was obtained from all subjects. Family 2 was part of a kindred previously reported[2].

Genetic analysis. Samples were genotyped at deCODE Genetics (Reykjavik, Iceland). Twelve polymorphic markers at 0.04–1.6-cM intervals covering the previously reported CMT2C region[5] were used for fine mapping. Multipoint parametric and nonparametric analyses and haplotype reconstruction were done using Genehunter 2.0[32] and Simwalk2 v2.91[33]. Mendelian inconsistencies were checked using PedCheck (version 1.1); genotyping data was formatted for Simwalk2 using mega2 (v4.0), and haplotypes were visualized using HaploPainter (v.029.5). SNP array analysis (Illumina Infinium II HumanHap550K SNP chips BeadStation v2.3.25, Illumina Inc.) was performed using DNA samples from one affected individual from families 1 and 2.

qRT-PCR. RNA was isolated from human lymphoblast cells, spinal cord and tracheal cartilage (Maryland Brain and Tissue Bank) using Trizol (Invitrogen) and converted to cDNA using High Capacity cDNA RT kit (Applied Biosystems). PCR reactions were run using TRPV4 and glucoronidase (hGUS) primers (ABI) and the ABI Prism 7900 Sequence Detector System as described[34].

Expression of TRPV4 in mammalian cells and *Xenopus* oocytes. Constructs (pcDNA3.1, pcDNA3.1-Flag and pcDNA3.1-YFP) expressing human *TRPV4* cDNA were provided by M.A. Valverde (Department of Experimental and Health Sciences, Universitat Pompeu Fabra, Barcelona, Spain)[11]. R269C, R269H and M680K mutants were generated using QuickChange (Stratagene). For expression in *Xenopus* oocytes, TRPV4 cDNA constructs were obtained by PCR of mouse kidney cDNA and inserted into pTLB. These cDNAs were subcloned into a modified pIRES-CD8 for mammalian cell transfection. HEK293, HeLa and DRG cells were transfected using Lipofectamine 2000 (Invitrogen) or polyethyleneimine in Optimem (Invitrogen). Cell surface expression of TRPV4 was determined by incubating transfected cells with SulfoLink NHS Biotin (Pierce) for 1 h at 4 °C. Post-nuclear supernatant was incubated with streptavidin agarose for 60 min at room temperature. Beads were pelleted, washed and protein recovered by heating with reducing loading buffer. 5% input and half of the biotinylated protein were separated on 4–12% SDS gels using MOPS buffer (Invitrogen) and visualized by protein blot using antibody to TRPV4 (anti-TRPV4; Sigma no. T9075) and mouse anti-actin (Sigma).

Immunohistochemistry. Cells were transfected and fixed with 4% paraformaldehyde (PFA)/0.05% NP-40 detergent. Trpv4-null and wild-type littermate mice were transcardially perfused with 4% PFA. Spinal cords were cut into 50-µm cryostat sections. Antibodies used were rabbit anti-TRPV4 (Sigma), rabbit anti-TRPV4 (ref. 15), rabbit anti-TRPV4 (gift from S. Heller, Department of Otolaryngology—Head and Neck Surgery, Stanford University School of Medicine, Stanford, California), monoclonal anti-TRPV4 (Alomone), rabbit anti-Flag (Abcam), monoclonal anti-calnexin (Becton Dickinson), acetylated tubulin (Sigma), goat anti-choline acetyltransferase (Chemicon) and secondary antibodies conjugated to Alexa Fluor 488, 546 or 594 (Molecular Probes). Images were obtained using Zeiss LSM-510 META confocal microscope.

Cell death assays. DRGs[35] were transfected with TRPV4 pcDNA3.1-YFP constructs, harvested in PBS-10% serum containing 25 µg/ml propidium iodide (PI; Sigma), and sorted using FACSCalibur Flow Cytometer and CellQuest Pro software (BD Biosciences) recording ≥50,000 events. Percent cell death was the percentage of YFP/PI double-positive cells.

HEK293 cells were transfected with TRPV4 pcDNA3.1-Flag constructs using 0.1 µg of TRPV4 plasmid and 0.4 µg empty vector per well of a 24-well plate. Ruthenium red (10 µM; Sigma) or RN1734 (10 µM) was added 4 h post-transfection. At 24 h or 48 h, cells were incubated with 2 µM calcein AM and 4 µM EthD-1 (Molecular Probes) and imaged using Zeiss AxioImager Z1 microscope. Dead cells (red) and live cells (green) were counted using Zeiss Axiovision 4.6 software. Equal expression of TRPV4 was confirmed by protein blot of cells transfected under identical conditions.

Calcium imaging. HEK293 cells were transfected with human TRPV4 and the fluorescent marker mCherry. Cells were replated onto polyornithine-coated coverslips 4.5 h after transfection and maintained at 37 °C and 5% CO_2. Ruthenium red (10 µM) was added at the time of replating. Calcium imaging was done at 22–24 h[15].

Plate-based intracellular calcium assay. Intracellular calcium levels were determined using a calcium assay kit according to manufacturer's instructions (no. R8041, Molecular Devices). HEK293 cells were transfected. At 4 h, RN1734 was added at 10 µM. At 24 h, media was removed, 50 µl of Calcium Assay Reagent was added, and cells were incubated at 37 °C for 1 h. Fluorescence was quantified using a fluorescent imaging plate reader (FLIPR, Molecular Devices).

Electrophysiology. Mouse TRPV4 cRNA was transcribed from pTLB constructs. 0.5–5 ng was injected into oocytes incubated in nominally Ca^{2+}-free solution. Whole-cell membrane currents were measured using an npi Tec01 TEVC amplifier (npi, Tamm). Currents were activated by increasing temperature using a Peltier-based solution cooler/heater (CL-100, Harvard Apparatus) or by preincubation with 5 µM 4αPDD (LC laboratories) for 30 min. Temperature-activated currents were measured initially and when the bath had reached 38 °C (see **Fig. 3b**, points 1 and 3). Preincubation with 4αPDD rather than acute application was used due to the observed slow activation of TRPV4 currents in oocytes. A ramp or pulse protocol was used in clamping oocytes from −100 to +100 mV, and currents were compared at −100 mV. Each experimental condition was replicated in at least 3–4 different oocyte batches. Recordings were performed in a solution containing 100 mM sodium gluconate, 20 mM calcium gluconate, 4 mM $MgSO_4$ and 5 mM HEPES, pH 7.5.

HEK293 cells were transfected as described with addition of pNEGFP for visual selection of transfected cells. Whole-cell currents were measured at 25 °C with Axopatch 200B (Molecular Devices) using a repeated ramp protocol (−100 to +100 mV, 400 ms, every 2 s). The solutions were: standard extracellular, 150 mM NaCl, 5 mM KCl, 1 mM $MgCl_2$, 2 mM $CaCl_2$, 10 mM glucose, 10 mM HEPES, pH 7.4 with NaOH; hypotonic (200 mOsm), NaCl reduced to 80 mM; isotonic (320 mOsm), 120 mM mannitol added to hypotonic solution; and pipette solution, 140 mM CsCl, 5 mM EGTA, 10 mM HEPES, pH 7.2 with CsOH.

Protein structure determination. TRPV4-$ARD_{132–383}$ was purified as described[21]. TRPV4-ARD crystals were grown in hanging drops at 4 °C in 0.1 M sodium citrate pH 5.0, 10% MPD, 2% PEG8000, 4.3% trifluoroethanol and frozen in reservoir with 20% PEG4000 (crystal form I), or 0.025 M KH_2PO_4, 7% MPD, 7% PEG8000, and 5 mM DTT and frozen in reservoir with 25% PEG400 (crystal form II). Data were collected at 110 K and 1.54 Å on a Micromax007/R-AXIS IV++ (Rigaku/MSC Inc) and processed with HKL2000. Structures were determined by molecular replacement using TRPV2-ARD[22] as search model in MOLREP[36], model building in COOT[37], and refinement using REFMAC[38]. Data and refinement statistics are in **Supplementary Table 1**. Coordinates were deposited in the Protein Data Bank (3JXI and 3JXJ are crystal forms I and II, respectively).

Co-immunoprecipation. HEK293 cells were cotransfected with pcDNA3 expressing human PACSIN1, PACSIN2 or PACSIN3 (gifts of M. Plomann, Cellular Neurobiology Research Group, Center for Biochemistry, University of Cologne, Cologne, Germany) and Flag-TRPV4. At 24 h, cells were harvested and cleared and cell lysates were incubated with anti-Flag M2 (Sigma) for 6 h followed by overnight incubation with Dynabeads Protein G (Dynal). The beads were washed, and bound proteins were separated by SDS-PAGE and analyzed by immunoblotting with antibodies to PACSIN3, PACSIN2 and PACSIN1 (gifts of M. Plomann), respectively. TRPV4 imunoprecipitation was verified by immunoblotting with anti-Flag M2.

Protein binding assays. Wild-type and mutant human TRPV4-ARDs, including the N-terminal proline-rich region (residues 136–397), were

expressed and purified as the chicken Trpv4-ARD. Mouse Pacsin3-Sh3 domain (residues 361–424; single difference between mouse and human PACSIN3-SH3 is V362A; cDNA provided by S. Heller) was cloned into NdeI and NotI sites of pET21-C6H, expressed in BL21 (DE3) cells induced with 0.4 mM isopropyl-β-D-thiogalactopyranoside at room temperature. Cells were lysed by sonication in lysis buffer (20 mM Tris-HCl, pH 8.0, 300 mM NaCl, 20 mM imidazole, pH 7.0, and 1 mM phenylmethylsulfonyl fluoride) with 0.1% Triton X-100, 0.2 mg/ml lysozyme, 50 μg/ml RNase A and 25 μg/ml DNase I. The cleared lysate was loaded onto Ni-NTA (Qiagen) and eluted with steps of 25, 50, 100, 150 and 250 mM imidazole pH 7 in lysis buffer, adding 10 mM EDTA at pH 8.0 and 1 mM dithiothreitol (DTT) after elution. Relevant fractions were pooled, dialyzed, purified on Superdex75 (GE Healthcare) in 10 mM Tris-HCl, pH 8.0, 50 mM NaCl, 1 mM DTT, and concentrated to >20 mg/ml in centrifugal filters. For PACSIN3-SH3 interaction assays, samples contained 25 nmol TRPV4-ARD with or without 37.5 nmol PACSIN3-SH3 in 125 μl pre-incubated for >30 min, and 100 μl were loaded onto a Superdex75 10/30 column (GE Healthcare) in 20 mM Tris, pH 7.0, 150 mM NaCl, 1 mM DTT at 4 °C. Calmodulin-agarose binding assays were performed essentially as described[21].

Statistics. Data were analyzed using Excel (Microsoft) and the Strathclyde electrophysiology suite (Unive. Strathclyde). Statistical significance was determined using paired or unpaired Student's *t* tests where appropriate.

32. Kruglyak, L., Daly, M.J., Reeve-Daly, M.P. & Lander, E.S. Parametric and nonparametric linkage analysis: a unified multipoint approach. *Am. J. Hum. Genet.* **58**, 1347–1363 (1996).
33. Sobel, E., Sengul, H. & Weeks, D.E. Multipoint estimation of identity-by-descent probabilities at arbitrary positions among marker loci on general pedigrees. *Hum. Hered.* **52**, 121–131 (2001).
34. Avila, A.M. *et al.* Trichostatin A increases SMN expression and survival in a mouse model of spinal muscular atrophy. *J. Clin. Invest.* **117**, 659–671 (2007).
35. Chen, W., Mi, R., Haughey, N., Oz, M. & Hoke, A. Immortalization and characterization of a nociceptive dorsal root ganglion sensory neuronal line. *J. Peripher. Nerv. Syst.* **12**, 121–130 (2007).
36. Vagin, A. & Teplyakov, A. An approach to multi-copy search in molecular replacement. *Acta Crystallogr D Biol Crystallogr* **56**, 1622–4 (2000).
37. Emsley, P. & Cowtan, K. Coot. Model-building tools for molecular graphics. *Acta Crystallogr D Biol Crystallogr* **60**, 2126–2132 (2004).
38. Murshudov, G.N., Vagin, A.A. & Dodson, E.J. Refinement of macromolecular structures by the maximum-likelihood method. *Acta Crystallogr D Biol Crystallogr* **53**, 240–255 (1997).

doi:10.1038/ng.512